



Impact of Sample Geometry and Surface Finish on VM12-SHC Ferritic–Martensitic Steel Under Cyclic Steam Atmosphere Operating Conditions

M. Mosquera Feijoo¹ · G. Oder¹ · R. Saliwan Neumann¹ · M. Buchheim¹ · A. Kranzmann¹ · J. Olbricht¹

Received: 30 May 2021 / Revised: 8 May 2022 / Accepted: 10 May 2022
© The Author(s) 2022

Abstract

The steam side oxidation of ferritic–martensitic VM12-SHC steel was investigated under thermo-cyclic conditions in water steam at 620/320 °C and 30 bar with a focus on assessing the influence of pre-oxidation time, specimen geometry and surface finish. The specimens were pre-oxidized under isothermal conditions in water steam at 620 °C and 30 bar for 500 h or 1500 h. After pre-oxidation treatment, all specimens were subjected up to 258 thermal cycles. Three different geometries—rectangular coupons, U-shaped ring segments and ring samples—were investigated to evaluate the influence of open/closed shape, and flat/curved surface on corrosion rate. At the same time, two types of surface finish were considered: “as received” and “ground.” The formation of a protective scale by pre-oxidation was investigated. EBSD and ESMA analyses revealed that the Cr-content of the alloy appeared to be insufficient for obtaining a protective oxide scale under studied conditions, at the same time the analyses confirmed that initial oxidation depends on presence of minor alloying elements as Si and Mn, strong oxide formers which can alter the kinetics and morphology of the corrosion reaction. Moreover, rectangular coupons with small wall thickness and flat surface exhibited the highest corrosion rate, while “ground” curved samples showed only local oxidation. This indicates that for same pre-oxidation time, oxidation kinetics is controlled by curvature.

Keywords Cyclic steam oxidation · 12%Cr steel · Specimen geometry · Surface treatments

✉ M. Mosquera Feijoo
m.mosquera.feijoo@gmail.com

¹ German Federal Institute for Materials Research and Testing (BAM), Unter den Eichen 87, 12205 Berlin, Germany

Introduction

Steam power plants operate at varying temperatures due to changing demands (day/night, summer/winter, outages...); this implies that testing of materials in operating power plants is necessary in order to come near the real operating conditions and the materials are exposed to realistic conditions (pressures, temperatures, load cycles) [1]. Moreover, in the development phase of ferritic–martensitic chromium steels, the focus was on the mechanical properties of these steels, but when taking them to practical operation conditions, it turned out that much of the life time of the materials and components is determined by their oxidation properties [2]. Steam oxidation resistance is required as otherwise, at temperatures higher than 600 °C, the resulting thick oxide scales will spall, causing blockage of tube bends as well as overheating of heat exchangers due to a thermal insulation effect, erosion of downstream components and loss of cross section in critical components [3].

It is well known that high-temperature oxidation in 100% steam is characterized by faster oxidation rates than in dry or humid environments [4]; in addition, the scale formed exhibits different adherence and porosity [5, 6] leading to a loss of the protective properties of chromia scale [7]. Under cyclic conditions, the oxidation resistance of ferritic–martensitic steels depends primarily on their chromium content and the rapid formation of a dense protective Cr-rich oxide scale. The oxide scales formed at high temperatures are generally subject to mechanical stresses, which can arise from the oxide growth process itself, or, on the other hand, as a consequence of stresses acting on the material [8]. If the alloy chromium concentration is high enough, growth of a protective, chromium-rich oxide scale is sustained under isothermal conditions, and its regrowth after mechanical damage is supported [9].

However, it was observed that the behavior of a chromium containing steel in experimental environment differs from the data obtained in real service life where metal is in contact with steam [10], these differences are not well understood [11]. In general, oxide characterization studies in laboratories use polished or ground coupons and the sample surface as well as the arising oxide scale differ from those formed on components of a real power plant. The heat exchanger tubes are not polished, and their geometry (curved and close shape) is very different from the rectangular coupons (flat surface and edges) used in laboratory tests. Therefore, in addition to Cr-content and temperature, factors as sample geometry and finish surface have an impact in the oxidation kinetics and oxide scale morphology [12–19]. The growth of oxides on curved substrate surfaces leads in many cases to “growth stresses,” which do not occur on flat surfaces and therefore arise from the geometry. Sufficient amounts of chromium must be supplied by fast diffusion to the steel surface [20], and the diffusion can be enhanced by surface treatments [21–25]; surface deformation, e.g., by grinding, creates a high density of dislocations that act as fast diffusion paths for metal and enhances the diffusion of the selectively oxidized elements Cr, Si and Mn, favoring the formation of a Cr-rich protective oxide [20]. The importance of minor elements on the

steam oxidation such as Si, Co, Mn, Mo and W has been reported, indicating that the critical Cr content of the alloy required to form a protective oxide depends on the presence of these minor alloying elements, as well as the microstructure and the service temperature [26].

Based on existing data reported by Ennis et al. [27], the main factors to consider for the evaluation of studied materials under cyclic conditions are the loss of material, depletion zone in the matrix, and oxides spall during service. The purpose of this paper is to explore the combined effects of sample geometry (wall thickness, open/closed shape and flat/curved surface) and finish surface (as received/ground) on the stability of oxide scale and formation of protective oxides in 12%Cr content alloy under cyclic steam oxidation, simulating the in stationary operation of steam-cycle power plants.

Experimental Procedures

Heat exchanger tubes of VM12-SHC steel (nominal composition Fe-0.1C-0.5Si-0.4Mn-11.2Cr-0.2Mo-0.3 V-1.7Co-0.2Ni) were manufactured by Vallourec Tubes France as a tube with an outer diameter of 38 mm, inner diameter of 28 mm and, consequently, a nominal wall thickness of 5 mm. The samples were cut into rectangular coupons (15 mm × 10 mm × 4 mm), U-shaped segments (10 mm wide) and rings (20 mm wide) as illustrated in Fig. 1. Two types of specimens were considered: as received (raw samples carrying the technical surface from tube production) and ground samples. In the case of “ground” samples, before the exposure, the inner face of U-shape and rings were mechanically ground to remove the existing oxides on the surface. The average surface roughness (R_a) measured on five independent lines (length 2 mm) was 0.6 μm in rectangular coupons (Profilometer Polaris MFC (Model 08, 1999)), and for U-shape and ring samples, the average surface roughness of the inner surface was 0.5 μm (Profilometer Microprof TTV, FRT). Prior to oxidation, all samples were cleaned with ethanol and dried at room temperature. All samples were weighted and measured to determine the surface area exposed to the oxidative environment.

Corrosion tests were carried out in two test rigs with horizontal tube furnaces specially designed for this study, one equipment for isothermal pre-oxidation treatment and a second equipment for cyclic condition (Fig. 2). Both equipments involve

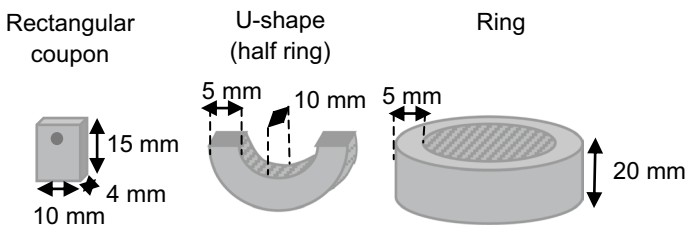


Fig. 1 Geometry and dimensions in mm of the experimental samples obtained from VM12-SHC tube

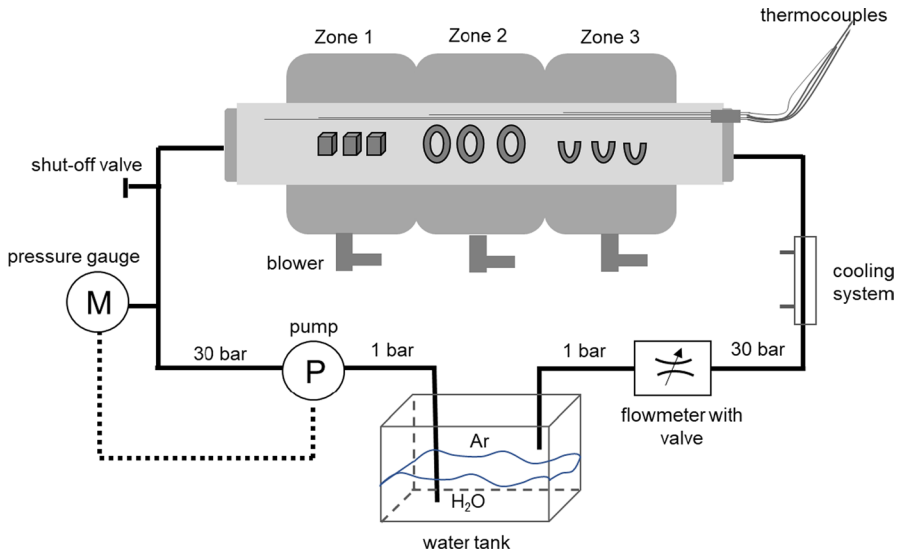


Fig. 2 Schematic diagram of the steam oxidation system facility for coupon experiments with temperature cycles

furnaces with three heating zones, and in case of the cyclic test rig forced air cooling ensured the rapid cool-down of the furnace and the steam-filled and pressurized reactor. The flowing steam was generated by pumping ultra-purified water into the pre-heating device, at the flow rate is 8 ml/min and 30 bar of pressure. The samples were placed in alumina crucibles to ensure the collection of oxide spalls and a proper data assessment. A first experiment with rectangular coupons was carried out; the heat treatment consisted in an initial isothermal treatment for 500 h at 620 °C and 30 bar followed to cycling condition with a temperature range of 620° /320 °C up to 258 cycles at 30 bar in water steam (Fig. 3). Due to the absence of a continuous oxide scale on rectangular coupons after the experiments, no breakaway occurred. The pre-oxidation time was increased up to 1500 h in a second experiment; after this time, the nodules cover the whole surface and lead to a continuous

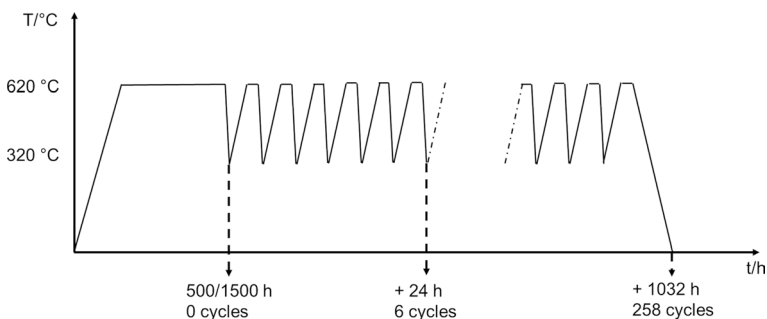


Fig. 3 Temperature and time profile used for oxidation experiments







oxide scale. During all experiments, the temperature was recorded with a custom-built acquisition system based on Labview software. Each temperature cycle lasted 4 h (60 min heating + 60 min holding + 90 min cooling + 30 min holding). Three coupons of each geometry and surface finish were removed during planned interruptions after pre-oxidation, 6 cycles, 30 cycles, 96 cycles, 180 cycles and 258 cycles for examination. Table 1 summarizes the different geometries and surface investigated in this study.

Before and after the oxidation experiments, all coupons were weighted to evaluate the mass changes. No spalled oxides were found after each cycle interval. The morphology of oxide scales was characterized by optical microscopy (Olympus Model GX71). The software LAYERS Version 1.7.1 was used to determine the total oxide scale thickness, material loss and porosity of the oxide scales on a metallographic cross section; the phase composition was identified by scanning electron microscopy SEM (LEO Gemini 1530VP, ZEISS), equipped with an energy-dispersive X-ray spectrometer (EDX) XFlash Detector 5030 and an electron backscatter diffraction (EBSD) detector e-Flash^{HD} (Bruker). Diffusion of oxygen and the distribution of chromium, manganese and silicon in the oxide scales and substrate were analyzed by a high-resolution microprobe EPMA (JEOL JXA-8900 RL).

Results and Discussion

In order to determine the influence of surface finish on the integrity of the oxide scales under cyclic corrosion in water steam, two surface finishings were studied: without surface treatment – later on designated as “as received” samples-, and “ground” samples- (Fig. 4). The EPMA results of the not oxidized samples indicate Fe-rich oxides with high Cr/Mn content, suggesting that spinel phases of type $(\text{Cr,Fe})_2\text{-O}_3$ and $(\text{Cr,Mn})_3\text{-O}_4$ are present in the existing oxide layer of “as received”

Table 1 Summary of sample geometries and surface treatments evaluated in this study

Experimental condition	Surface treatment	Pre-oxidation up to 258 cycles			
		500 h pre-oxidation up to 258 cycles	1500 h pre-oxidation up to 258 cycles		
Water steam 30 bar 620° / 320 °C	“ground”	Rectangular coupon 	Rectangular coupon 	U-shape 	Ring 
	“as received”			U-shape 	Ring 

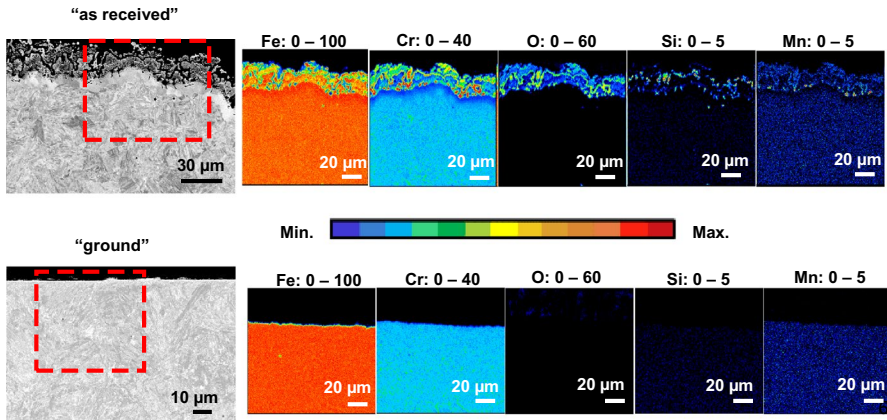


Fig. 4 EPMA mappings showing the local distribution of major constituting elements in wt.% for VM12-SHC base material in the **a** "as received" **b** "ground" condition at the inner surfaces of the tubes, prior to the oxidation tests

samples (Fig. 4). The microstructure of VM12-SHC is a tempered martensite with carbides distributed in the matrix, responsible for its creep life [20]. During manufacturing process, all Cr carbides in the near-surface material layer are dissolved, and Cr is absorbed into the oxide layer. In addition, the layer is decarburized. As a result, the lath-type martensitic microstructure becomes unstable and ferrite is formed. As consequence, a depletion zone of Cr, Fe and Mn with a thickness of around 10 μm is found underneath the oxide scale. A corresponding layer with a coarse-grained microstructure can be observed in the respective micrograph (Fig. 5), whereas the bulk material on the left and center of the image shows traces of the typical

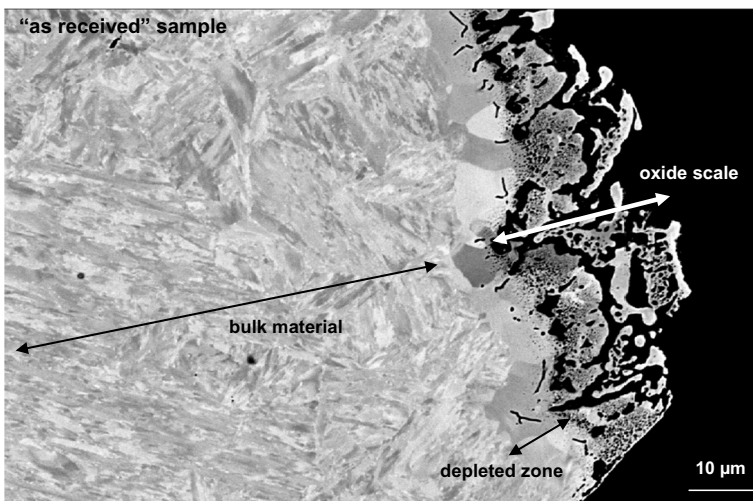


Fig. 5 EPMA micrograph of the cross section of an "as received" sample prior to oxidation

“martensitic” microstructure of VM12-SHC. However, due to the depletion of Cr, Mn and Si, the substrate shows the transformation of martensitic to ferritic microstructure adjacent to the substrate-scale interface (internal oxidation zone). Figure 5 also demonstrates a special morphology of the oxide scale in the as received condition, which is characterized by delamination, a high degree of porosity and/or cracks that might result from high temperature forming steps during processing.

According to Ennis et al. [28], if a thermal cycle is introduced in the early stages of the oxidation process, the poor adherence caused by the presence of gaps results in spallation of the outer scale; therefore, to minimize the impact of voids and pores formation, all samples of the present study were pre-oxidized under isothermal conditions. A first experiment was carried out with rectangular coupons at 620 °C and 30 bar under water steam for 500 h, but due to the absence of a complete oxide layer the pre-oxidation time was increased up to 1500 h. Figure 6 shows the comparison of surface and cross-sectional images of rectangular coupons after pre-oxidation treatments (500 h and 1500 h), and after 258 temperature cycles between 320 °C and 620 °C. Significant differences in the morphology of the oxide scales grown under different pre-oxidation time can be observed. SEM images of the surfaces reveal that after 500 h of pre-oxidation treatment, Fig. 6a, oxide nodules but also scratch marks from the surface preparation are still observed, which indicates a very thin oxide scale. The cross section confirms local oxidation (oxide nodules) even after 258 cycles (Fig. 6b). After 1500 h of pre-oxidation, the image in Fig. 6c reveals a uniform oxide layer with big oxide grains covering the surface and the presence of cracks; the cross section shows a duplex oxide layer with an internal oxidation zone—a mix of oxides and substrate—at the oxide scale/substrate interface. After 258 cycles, the oxide morphology on the surface becomes finer. Extended cracks are observed, and the cross section indicates no increase in the oxide scale thickness.

Porosity content is reduced after 258 cycles in both oxide scales (Fig. 6c and d), but gaps are observed at the interface of outer/inner oxide layer of oxide nodules

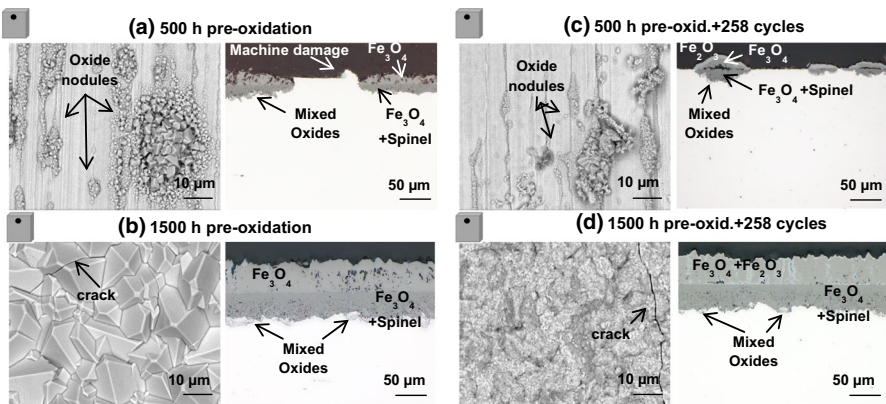


Fig. 6 Surface morphologies and cross sections of oxide scales of rectangular coupons exposed to water steam: **a** 500 h of pre-oxidation and **b** 1500 h of pre-oxidation at 620 °C and 30 bar, **c** 500 h pre-oxidation and 258 cycles and **d** 1500 h pre-oxidation and 258 cycles at 620°/320 °C and 30 bar

(Fig. 6c), which might enhance the spallation of the oxides. EBSD analyses reveal the same oxide phases on both coupons after 500 h (Fig. 6a) and 1500 h (Fig. 6b) of pre-oxidation time. After 258 temperature cycles, the phase composition appears to be modified: Fe_2O_3 is detected on the top of the oxide scale of both samples (Fig. 6c, d) and penetrating the outer magnetite layer in Fig. 6d, indicating high oxygen activity due to crack formation in the outer oxide scale.

Since the extended pre-oxidation time of 1500 h proved to yield satisfactory results, the remaining sample geometries, U-shape and rings, were exposed at the same experimental conditions as rectangular coupons, 1500 h of pre-oxidation and 258 cycles. It is well known that for steels with a Cr content between 9–12%, the oxidation rates and scale morphologies may substantially differ as function of time, temperature, minor alloying additions and surface treatment [25]. Therefore, the impact of the geometry was investigated using samples with open/closed shape (U-shape/ring), flat/curved surface and wall thickness (coupon/U-shape and ring), and the surface finish was again evaluated through “ground”/“as received” samples. Figure 7 presents the weight change as a function of oxidation time in water steam at 30 bar up to 258 cycles for all coupons, with the oxidation time plotted on a logarithmic scale. All mass change curves show that the oxidation of VM12-SHC samples follows the parabolic rate dependence. Fast reaction was found for rectangular coupons pre-oxidized for 1500 h that exhibit the largest mass increase. Analyses of the oxide thickness demonstrated that rectangular coupons (1500 h pre-oxidation) exhibit an oxide scale even thicker than “as received” U-shape and ring samples. It can be supposed that rectangular coupons overestimate the oxidation kinetics, maybe because they create an active surface and as result, the chemical gradient can be quickly created. After 1500 h of pre-oxidation and 258 cycles, the corrosion rate observed in curved “ground” samples behaves very differently than the observed in rectangular coupons. In case of rectangular coupons, the flat surface promotes a

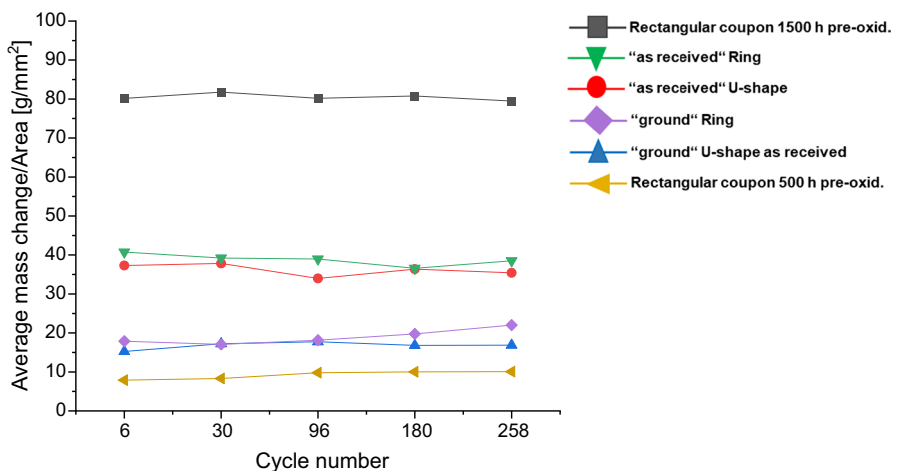


Fig. 7 Mass change during cyclic oxidation of the different geometries and finishing surfaces in water steam atmosphere at 30 bar, displayed as a function of cycle number plotted on a logarithmic scale

faster diffusion compared to curved surface of U-shape and rings. At the same time, it was found that mass change varies with the finishing surface, “as received” samples exhibit more mass increase than the “ground” samples.

The size of the oxides varies with the surface finish, as illustrated in Fig. 8. After 258 cycles “ground” U-shape exhibits local oxides on the surfaces (Fig. 8b), the same oxide morphology with nodules and thin layer as observed in rectangular coupons after 500 h of pre-oxidation. This indicates that 1500 h of pre-oxidation is not enough to develop a continuous oxide layer in “ground” U-shape and rings. However, after pre-oxidation treatment “as received” U-shape was covered with a continuous oxide layer (Fig. 8a). In addition, it is observed that scales of both finishes show mechanical damage, cracks, gaps, due to porosity and voids. Although the scales are cracked and porous, they remained adherent to the metal. Oxide spalls were not found after the experiments.

Figure 9 shows the comparison of cross-sectional images of “ground” and “as received” samples after 258 cycles in water steam at 30 bar. Rectangular coupon pre-oxidated for 500 h and ground U-shape and ring samples exhibits local oxidation, developing nodules growing through a thin oxide layer. However, rectangular coupons pre-oxidized for 1500 h and “as received” U-shape and ring exhibit a thick corrosion scale, which consist of a duplex oxide scale. As indicated by a white dashed line in Fig. 9, the effect of finishing surfaces can be observed through cross sections, outer and inner oxide scales are well distinguished in “ground” samples by a flat line, while in case of “as received” samples that interface is discontinuous. Identification of oxide phases was done by EBSD. It was found that in all samples the oxide scales are composed of same oxide phases, an outer layer composed of Fe_2O_3 and a middle layer of Fe_3O_4 , and an inner two-phase layer of $\text{Fe}_3\text{O}_4 + \text{Fe}_x\text{Cr}_y\text{O}_4$ spinel. There are traces of Fe_2O_3 in the outer Fe_3O_4 layer and at the outer/inner oxide scale interface of the rectangular coupon, which indicates the presence of cracks. All scales exhibit a compact outer layer of Fe_3O_4 with an inner oxide scale that contains much porosity. In real service conditions, Fe_2O_3 and Fe_3O_4 have maximum stability, but these oxides have a large

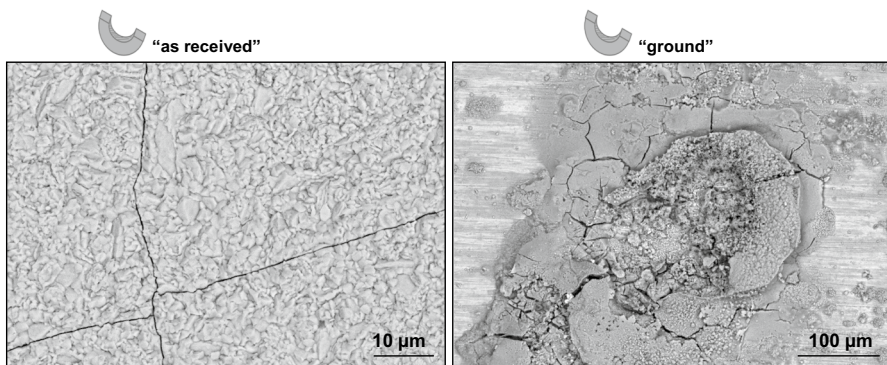


Fig. 8 Surface morphologies of oxide scales of U-shape sample exposed under water steam at 30 bar **a** “as received” after 1500 h of pre-oxidation and 6 cycles, and **b** “ground” after 1500 h of pre-oxidation and 258 cycles

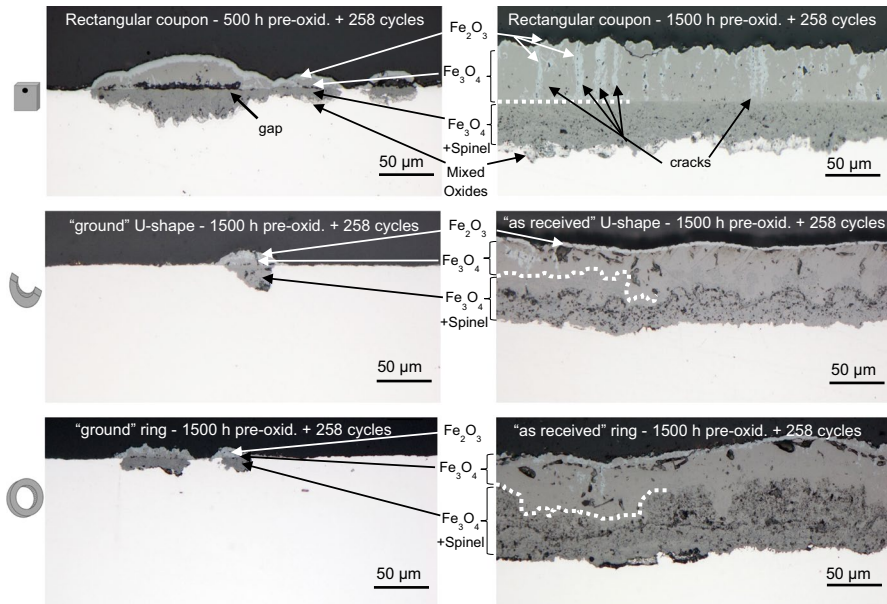


Fig. 9 Cross sections of oxide scales of rectangular coupons, U-shaped ring segments and ring samples exposed to water steam up to 258 cycles and 30 bar

number of structural defects [10]. However, a difference at the metal-oxide interface is also observed, since the coupons show stronger internal oxidation compared to curved samples.

The impact of finishing surface becomes clear from the images of Fig. 9 and confirms the importance of studying the changes of the microstructure of the base metal at the subsurface due to the machining preparation. It is reported that the subsurface dislocations generated by typical polishing processes promote chromium diffusion and the formation of a chromia layer during the very first instants of high temperature exposure in a stainless steel with 18% Cr content, but subsequently as the manganese diffusion coefficient in chromia is higher than that of chromium, the formation of a Cr-Mn spinel oxide top layer was observed [29]. A minimum requirement for an Fe-Cr alloy to resist breakaway is that it be capable of forming a protective chromia scale under isothermal conditions. In case of “ground” samples—U-shape, ring, and rectangular coupons pre-oxidized for 500 h—detection of Mn and Si in the thin oxide layer between oxide nodules indicates the formation of a manganese containing oxide, based on calculation ternary equilibrium Fe-Cr-Si with O_2 the stable oxide phases are Fe_2SiO_4 and SiO_2 . A Cr depleted zone can be observed adjacent, no chromium was detected by EBSD analyses in this thin oxide layer, probably due to the comparatively low content of this element in VM12-SHC, which is not enough to develop a chromia phase under isothermal condition as shows EPMA mapping in Fig. 10. Even after 258 cycles, EPMA maps in Fig. 11 confirm the presence of Mn, Fe-spinel in the thin layer. In contrast to other available studies, e.g. [18], the material considered

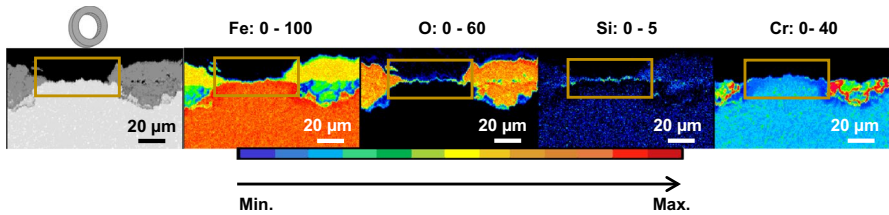


Fig. 10 EPMA mapping analysis in wt.-% of “ground” ring sample pre-oxidized for 1500 h in water steam at 620 °C and 30 bar

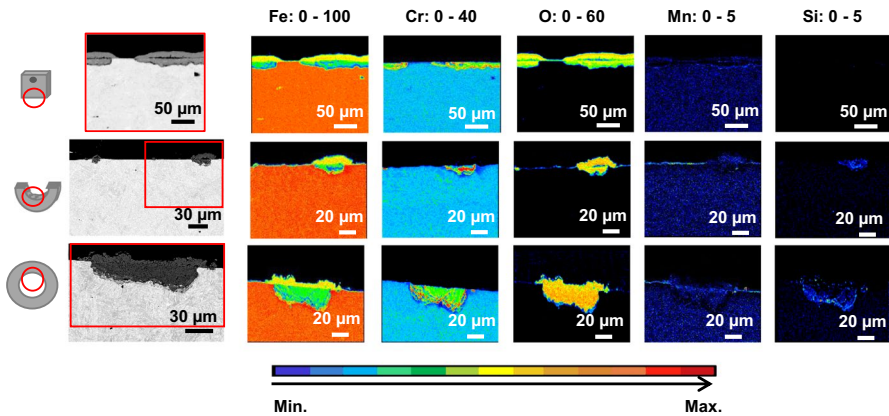


Fig. 11 Element mapping analysis in wt.-% of **a** rectangular coupon pre-oxidized for 500 h and 258 cycles, **b** “ground” U-shape pre-oxidized for 1500 h and 258 cycles, and **c** “ground” ring pre-oxidized for 1500 h and 258 cycles, in water steam at 30 bar

here with only 12% Cr is not able to form quickly enough a continuous chromia oxide layer at the beginning of the oxidation. Iron oxidation and a fast diffusion of manganese take place to the formation of Mn, Fe spinel oxide.

In case of “as received” samples, as observed in Fig. 9, the thick oxide scales contain many pores and cracks. According to Tuck et al. [29], porosity formation in the oxide scales is another mechanism which depends on the sample geometry; they observed that porosity on the exposed sample has been related to the geometry of the specimen in pure iron and low-alloyed steels; their investigations on pure iron and low-alloyed steels indicated compact scales with no porosity on flat surfaces; however, porous scales were formed on curved surfaces. This observation is confirmed for 12% Cr steel in the present study in Fig. 12. The porosity content was measured by the software Layers using optical microscopy images in samples with continuous oxide scales, and results indicate that a flat surface—rectangular coupons—contains the lowest porosity, whereas all curved surfaces yield higher values. The closed shape (ring) exhibits the highest porosity content of the three geometries.

If the scale becomes thick enough after pre-oxidation treatment and protective chromia is not formed, under cyclic conditions the scale can be damaged and

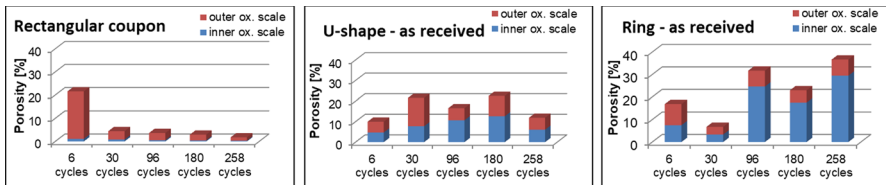


Fig. 12 Diagrams illustrating the porosity content in -% of oxide scales of rectangular coupons, U-shape and rings pre-oxidized for 1500 h after each cycle interval

rehealing deplete the alloy of chromium and failure can result [9]. Internal oxidation zone is strong after 6 cycles in ring sample, Fig. 13b, and this zone is a consequence of oxygen diffusion through the grain boundaries and laths and Cr depletion of surface substrate and its diffusion in the oxide scale. It is composed of oxides and substrate mixture; nevertheless, it seems to disappear with the increasing of cyclic exposure (Fig. 13d). This internal oxidation zone was analyzed by EPMA in Fig. 14. Maps reveal the chromium depletion in the substrate of different sample geometries. According to Schütze et al. [2] after continued Cr-depletion, eventually the Cr-rich spinel can no longer be sustained; as a result, Fe-rich oxides are subsequently formed and the repetition of this process leads to a Cr-rich multilayer microstructure in the inner part of the scale, as observed especially in the curved samples of the present study (Fig. 14). The curved surfaces form quite equivalent oxide layers and are clearly different from the oxide layer observed in coupon. Carbides distributed in the substrate may act as reservoirs for further Cr band formation or crack healing as suggested by Mogire et al. [30]. At the same time, it is confirmed that the Cr diffusion and therefore the formation of a protective oxide scale substantially depends on the presence of minor alloying elements such as Si, Mn and Co on alloy microstructure; Si and Mn are strong oxide formers and can alter the kinetics and morphology of the corrosion reaction. Studies have reported that Si significantly reduces the oxidation rate of Cr, whereas Mn seems to have the opposite effect [31, 32]. From other investigations, it can be expected that manganese can have a positive effect in water vapor containing environments by slowing down the evaporation rate of chromium

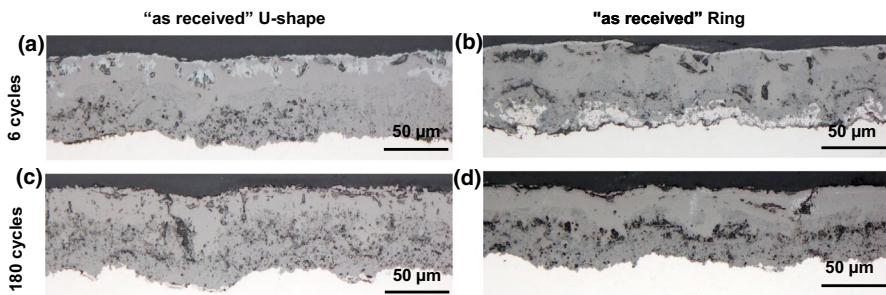


Fig. 13 Evolution of the internal oxidation zone in “as received” U-shape after: **a** 6 cycles, and **c** 180 cycles; “as received” ring-shapes after: **b** 6 cycles, and **d** 180 cycles, in water steam at 30 bar

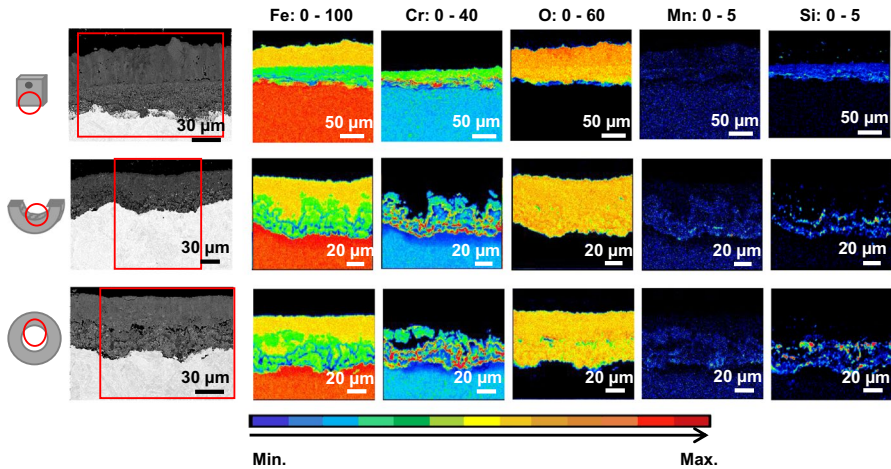


Fig. 14 Element mapping analysis in wt.% of **a** rectangular coupon, **b** “as received” U-shape, and **c** “as received” ring pre-oxidized for 1500 h and 258 cycles, in water steam at 30 bar

containing hydroxyl species due to the formation of an outer Cr-Mn-spinel layer [33], and in particular, silicon seems to have a beneficial effect in water vapor containing environments with regard to slowing down the chromium depletion rates in the metal subsurface zone and, thus, extending the time to breakaway oxidation significantly [2].

The detection diffusion of multiple oxide forming elements into the oxide scale, Fig. 14, results in considerable changes of the alloy composition within the depleted near-surface region of the samples, possibly involving the dissolution of carbides which typically stabilize the positions of grain boundaries and laths in the tempered martensite microstructure. Related microstructure changes in the substrate of “ground” and “as received” samples were observed in the present study SEM micrographs, Fig. 15. Dashed lines in the micrographs indicate regions directly below the oxide scale which are characterized by larger and more circular grains compared to the “martensitic” grain structure in the lower layers of the substrate. Based on the localized transition around oxides and the appearance in ground as well as as-received samples, it may be concluded that this microstructure modification is indeed related to the depletion of mentioned elements Cr, Mn and Si. It is not triggered by any mechanical or chemical impacts of the cutting and polishing process during preparation of the samples.

Regarding the above-mentioned depletion of chromium, it should be mentioned here that the formation of volatile Cr–O–H species can lead to so-called Cr evaporation during oxidation of Fe-based alloys with high Cr contents at high temperature levels. According to Holcomb [34], a partial pressure of $\text{CrO}_2(\text{OH})_2$ at 600 °C and 163 atm pressure of about 7.1×10^{-10} atm. Based on the experimental conditions of the current work, the highest partial pressure for other Cr-species calculated by Factsage – Database FactPS and FactSteel are the following:

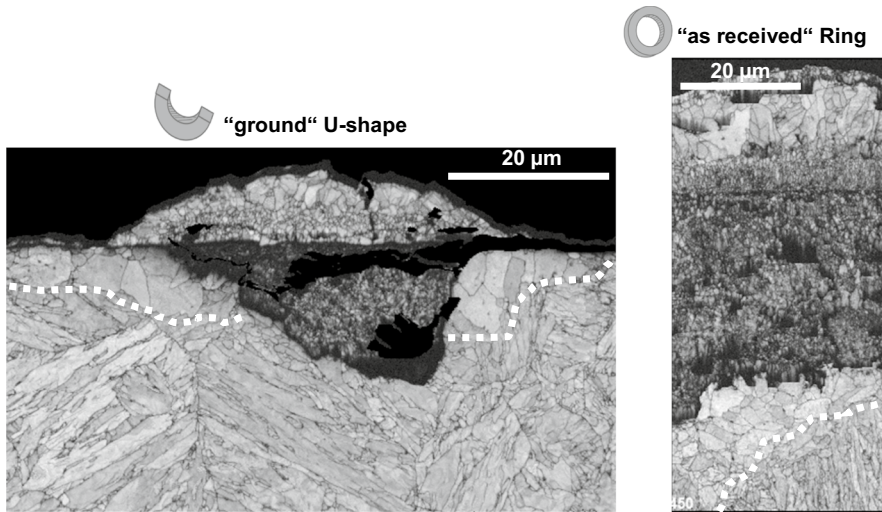
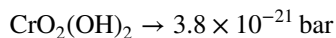
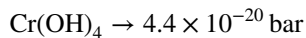
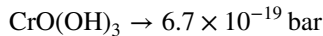
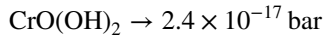
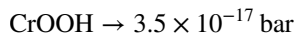
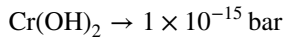
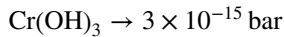


Fig. 15 SEM micrograph of the cross section of “ground” U-shape sample and “as received” ring sample after 258 cycles



In accordance with the above calculations, even the highest partial pressure of a Cr-species that is expected at 620 °C and 30 bar pressure is 5 orders of magnitude lower than in the condition Holcomb discussed, which in turn also means the Cr loss constant is roughly 5 orders of magnitude lower. Since our experiments had flowing but not fast flowing gas, and it may be assumed that the samples did not produce turbulent areas. Therefore, an influence of the shape in terms of formation of volatile Cr–O–H species can be neglected.

The mobility of chromium causes a very pronounced Cr depleted zone in studied samples as observed in previous element mapping analyses. EBSD analyses

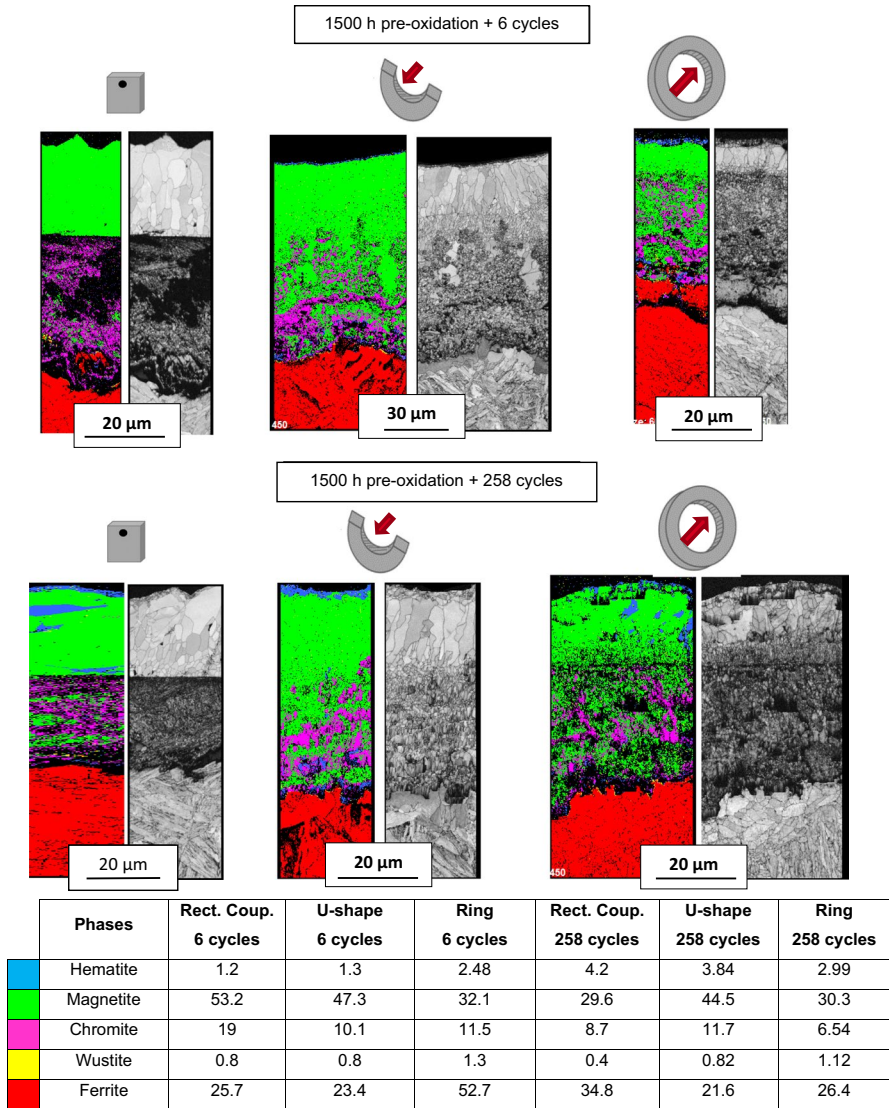


Fig. 16 EBSD analyses of “ground” rectangular coupons, U-shape sample and “as received” ring sample after 1500 h of pre-oxidation and **a** 6 cycles **b** 258 cycles

in Fig. 16 reveal the same oxide phases in rectangular coupon (ground), U-shape and ring samples (as received) after 6 and 258 cycles. This indicates the stability of oxide phases throughout the experiment, which confirms that the oxides formed on the “as received” surfaces and “ground” surfaces did not change (surface stays stable).

Results observed above demonstrate the importance of sample geometry and surface finish on the oxide growth mechanisms of VM12-SHC. The oxide scales of

investigated samples have a very different appearance. A pre-oxidation treatment of 1500 h should lead the formation of a multilayered oxide scale on “ground” samples; however, only rectangular coupons form a continuous oxide scale. This demonstrates the influence of the geometry—flat/curved surface—on oxidation kinetics. Additionally, a surface finish treatment seems to be favorable to develop local oxides up to 258 cycles, but formation of a protective scale is not observed under studied conditions. Changes of the microstructure in the matrix due to diffusion of alloying elements and oxidation processes are observed in all samples; this indicates damage in the substrate, which might promote creep damage.

Conclusions

In the present study, the cyclic steam oxidation behavior of VM12-SHC was investigated with a focus on the impact of sample geometries and surface finish of laboratory specimens. The following conclusion can be drawn:

- Formation of a continuous oxide scale in VM12-SHC under isothermal conditions in water steam depends on the combination of pre-oxidation time and geometry. For rectangular coupons, the pre-oxidation time was increased from 500 h up to 1500 h to obtain a continuous oxide scale which covers the surface. In case of curved samples, 1500 h is not enough to develop an oxide scale, which indicates the influence of sample shape (wall thickness and curved/flat surface) on the corrosion rate.
- The surface preparation and its geometry affect the oxidation behavior of VM12-SHC steel. The impact of the surface finish and curvature is reflected in the corrosion behavior under cyclic conditions. The corrosion rates of “ground” and “as received” samples differ considerably. In case of “ground” samples, rectangular coupons with flat surface promote a faster diffusion and therefore a formation of continuous oxide scale compared to “ground” curved shape that exhibits oxide nodules and a very thin oxide layer. Coupon specimen results tend to over-estimate the oxidation kinetics even after long exposure times (up to 2500 h in this study) and are therefore not representative for the oxidation behavior of curved components like heat exchanger tubes during cyclic steam oxidation.
- Oxide scales are multilayered formed Fe_2O_3 , Fe_3O_4 and $\text{Fe}_x\text{Cr}_y\text{O}_4$ spinel. Additionally, detection of Mn and Si in the inner oxide scales, as well as in the thin oxide layer observed between oxide nodules, suggest the presence of Fe_2SiO_4 and SiO_2 and Mn-spinel. The diffusion of Cr and alloying elements modifies the microstructure of the substrate underneath the oxide scale, from martensitic to ferritic, that might promote damage in the metal for longer exposition.
- The current findings indicate that more representative results may be obtained by oxidation testing of curved sections from heat exchanger tubes, like rings and U-shaped segments. The closed/open sample shapes yield similar results in terms of corrosion rate. Only the porosity content in the oxide scale is influenced by sample shape; rings (“closed” shape) exhibit the largest porosity content.

- No spallation was found, which indicates that oxide scales are well adhered to the substrate up to 258 cycles. Further investigations are required to determine the temperature conditions and cycle numbers up to which oxide spallation takes place.

Funding Open Access funding enabled and organized by Projekt DEAL. Bundesministerium für Bildung und Forschung, 03SF0474, Jürgen Olbricht.

Open Access This article is licensed under a Creative Commons Attribution 4.0 International License, which permits use, sharing, adaptation, distribution and reproduction in any medium or format, as long as you give appropriate credit to the original author(s) and the source, provide a link to the Creative Commons licence, and indicate if changes were made. The images or other third party material in this article are included in the article's Creative Commons licence, unless indicated otherwise in a credit line to the material. If material is not included in the article's Creative Commons licence and your intended use is not permitted by statutory regulation or exceeds the permitted use, you will need to obtain permission directly from the copyright holder. To view a copy of this licence, visit <http://creativecommons.org/licenses/by/4.0/>.

References

1. S. Straub and R. Knödler, in *10th Liege Conference: Materials for Advanced Power Engineering* (2014).
2. M. Schütze, M. Schorr, D. P. Renusch, A. Donchev, and J. P. T. Vossen, *Materials Research* **7**, 111 (2004).
3. T. U. Kern, K. H. Mayer, B. Donth, G. Zeiler, and A. DiGianfrancesco, *Materials for Advanced Power Engineering* **7** (2010).
4. T. Dudziak, M. Lukaszewicz, N. J. Simms, and J. R. Nicholls, *The International Journal of Corrosion Processes and Corrosion Control* **52** (2017).
5. J. Gabrel, C. Coussement, L. Verelst, R. Blum, Q. Chen, and C. Testani, *Material Science Forum* **369–372**, 931 (2001).
6. D. L. Douglas, P. Kofstad, A. Rahmel, and G. C. Wood, *Oxidation of Metals* **45**, 529 (1996).
7. A. Galerie, Y. Wouters, M. Pijolat, F. Valdivieso, M. Soustelle, T. Magnin, D. Deafosse, C. Bosch, and B. Bayle, Mechanisms of corrosions and oxidation of metals and alloys. *Advanced Engineering Materials* **3**, 555 (2001).
8. M. Schütze, *Protective Oxide Scales and Their Breakdown*. (Institute of corrosion and wiley, 1997). ISBN: 978-0-471-95904-5.
9. N. K. Othman, J. Zhang, and D. J. Young, *Corrosion Science* **52**, 2827 (2010).
10. G. M. Bakic, M. B. Djukic, B. Rajcic, V. S. Zeravic, A. Maslarevic, and N. Milosevic, *Structural Integrity Procedia* (2016).
11. R. K. Singh Raman, and B. C. Muddle, *International Journal of Pressure Vessels and Piping* **79**, 585 (2002).
12. M. Lukaszewicz, *Steam oxidation of advanced high temperature resistant alloys for ultra-supercritical applications*, (Cranfield University, PhD work, 2012).
13. D. Laverde, T. Gómez-Acebo, and F. Castro, *Corrosion Science* **46**, 613 (2004).
14. D. J. Young, J. Zurek, L. Singheiser, and W. J. Quadackers, *Corrosion Science* **53**, 2131 (2011).
15. Liu, *Journal of Power Sources* **179**, 286 (2008).
16. E. Essuman, G. H. Meier, J. Zurek, M. Hänsel, and W. J. Quadackers, *Oxidation of Metals* **69**, 2008 (143).
17. S. Guillou, C. Desgranges, and S. Chevalier, *Oxidation of Metals* **79**, 507 (2013).

18. M. R. Ardigo-Besnard, I. Popa, O. Heintz, R. Chassagnon, M. Vilasi, F. Herbst, P. Girardon, and S. Chevalier, *Applied Surface Science* **412**, 196 (2017).
19. S. Cissé, L. Laffont, B. Tanguy, M. C. Lafont, and E. Andrieu, *Corrosion Science* **56**, 209 (2012).
20. H. J. Grabke, Z. Tökei, and C. Ostwald, *Steel Research International* **75**, 38 (2004).
21. W. J. Quadakkers, and J. Zurek, *Oxidation in Steam and Steam/Hydrogen Environments*. (Oxford: Sheir's corrosion, Elsevier, 2010), p. 407.
22. Y. Madi, E. Shali, F. Charlot, A. Galerie, and Y. Wouters, *Oxidation of Metals* **75**, 167 (2011).
23. J. Yuan, X. Wu, W. Wang, S. Zhu, and F. Wang, *Oxidation of Metals* **79**, 541 (2013).
24. V. Tsisar, C. Schroer, O. Wedemeyer, A. Skrypnik, and J. Konys, *Journal of Nuclear Engineering and Radiation Science* **4** (2018).
25. C. Piehl, Z. Toেকেi, and H. J. Grabke, *Materials at High Temperatures* **17**, 243 (2000).
26. J. Zurek, L. Nieto Hierro, J. Piron-Abellan, L. Niewolak, L. Singheiser, and W. J. Quadakkers, *Materials Science Forum* **461–464**, 791 (2004).
27. P. J. Ennis and W. J. Quadakkers, *International Journal of Pressure Vessels and Piping* **84**, 82 (2007).
28. P. J. Ennis, and W. J. Quadakkers, in *Creep Resistant Steels*, eds. F. Abe, T. Kern, and R. Wiswanathan. (Woodhead Publishing Limited, Cambridge, 2008), p. S. 519
29. C. W. Tuck, M. Odgers, and K. Sachs, *Corrosion Science* **9**, 271 (1969).
30. E. O. Mogire, R. L. Higginson, A. T. Fry, and R. C. Thomson, *Materials at High Temperatures* **28**, 361 (2011).
31. H. E. Townsend, in *Proceedings of the International Corrosion Congress*. (Cape Town, 1999) (27.09.1999–01.10.1999, Proceedings, Paper 243).
32. R. J. Ehlers, and W. J. Quadakkers, *Report Forschungszentrum Jülich* (2001) (Jül-3883). ISSN 0944-2952.
33. H. W. Grünling, S. Leistikow, A. Rahmel, and F. Schubert, in *Aufbau von Oxidschichten auf Hochtemperaturwerkstoffen und ihre technische Bedeutung*, ed. A. Rahmel. (DGM, Oberursel, 1983), p. 7.
34. G. R. Holcomb, *Oxidation of Metals* **69**, 163 (2008).

Publisher's Note Springer Nature remains neutral with regard to jurisdictional claims in published maps and institutional affiliations.